V European Conference on Computational Fluid Dynamics
ECCOMAS CFD 2010
J. C. F. Pereira and A. Sequeira (Eds)
Lisbon, Portugal,14-17 June 2010

MODELLING OF ROUGHNESS-INDUCED TRANSITION USING LOCAL VARIABLES

Patrick Dassler*, Dragan Kožulović*, Andreas Fiala†

*Technische Universität Braunschweig
Institute of Fluid Mechanics
Bienroder Weg 3, D-38106 Braunschweig, Germany
e-mail: p.dassler@tu-bs.de
†MTU Aero Engines GmbH Germany
Dachauer Str. 665, D-80995 Muenchen, Germany
e-mail: andreas.fiala@mtu.de

Key words: Transition Modelling, Roughness

Abstract. *A new approach for modelling the roughness induced transition has been developed, which is based on local variables and a transport equation. Thus information of flow history relative to the considered point can be taken into account.*

The transported variable "Roughness Amplification" A_r serves as transition onset criterion. Two functions determining the value of A_r are implemented in this model. They generate A_r depending on several parameters like equivalent sand grain roughness height k_s and the dimensionless wall distance y^+ in close vicinity to the wall.

The model has been implemented in the DLR flow solver TRACE and has been validated by two test cases. The first test case is a flat plate with roughness and different linear pressure gradients. The second test case is also a flat plate but with a two-scale roughness. Results show the feasibility of this approach to the applied test cases and a good agreement with experimental findings.

1 INTRODUCTION

The distributed surface roughness exerts different effects at the flow. It increases the turbulent fluctuations in the turbulent boundary layer and it shifts the laminar-turbulent transition at some upstream position. Both effects increase the boundary layer losses and hence the drag forces, as reported by Schlichting[16] and Feindt[1], correspondingly. In contrast, the losses can also be decreased if the separation length of a laminar/ turbulent bubble is reduced or even completely prevented by enhanced transition tendency. Considering the laminar-turbulent transition process, the surface roughness can be regarded as one of the transition influencing parameters, like turbulence intensity, pressure gradients and Reynolds number, just to state some of them.

At large Reynolds numbers, where the boundary layer is almost completely in the turbulent state, the loss increasing mechanisms will prevail. Depending on the roughness dimensions and topology, the flat plate losses can be more than doubled[16]. According to Hummel[3], the loss coefficient ζ of a high Reynolds number turbine blade ($Re = 1\,200\,000$) is increased by 40 % by typical roughness structures, which usually occur after comparably small amount of gas turbine operation time.

At low Reynolds numbers the loss decreasing effect can be the dominant one. In particular, this effect is of interest for the low pressure turbine blades of jet engines operating at low Reynolds numbers ($Re < 100\,000$) during the cruise flight. Usually, the surface of the turbine blades is hydraulically smooth after the manufacturing process, but is roughened during operation such as from the equivalent sand grain roughness $k^+ < 1$ for the smooth surface to $k^+ > 5$ for a transitional-rough surface. Due to the aforementioned positive effect at the laminar separation bubbles, some low pressure turbine blades show even better performance after some time in operation.

The aim of the present work is to accurately predict the roughness effects at the laminar-turbulent transition process, yielding a suitable tool for the estimation of roughness effects. The effects at fully turbulent boundary layers are also accounted for by the approach of Wilcox[21], and will not be subject of additional modelling improvements herein. Furthermore, the single roughness elements will not be considered. The focus of the paper is at the distributed roughness only.

Different approaches are known for calculating the roughness-induced transition onset. Analytical methods determine the point of indifference occuring upstream of the transition onset. In that point disturbances in the boundary layer are neither amplified nor damped. Feindt[1] gave a correlation for determining the length between the point of indifference and the transition onset for different roughness heights. This can be implemented in semi-empirical transition models by the consideration of laminar boundary layer stability method approximation models, e.g. the e^N-method. In this approach the transition onset is achieved when the grown amplitude is e^N-times bigger than the initial amplitude, cf. Oertel and Delfs[11]. As proposed by Standish et al.[17], the roughness-induced transition can be taken into account by reducing the exponent N. Empirical

correlations on roughness height are also used for intermittency based transition models, cf. Stripf et al.[18],[19]. The physical intermittency describes the time-averaged turbulent proportion of the boundary layer. If the intermittency reaches one, the boundary layer is fully turbulent. Both the e^N and intermittency based method rely on integral boundary layer values, that means on non-local parameters.

2 MODEL FORMULATION

The transition model from Menter et al.[7],[8] deals with the intermittency concept described above. Instead of using boundary layer intregral values, this model uses only local variables. With this approach the transition can be calculated without determining the boundary layer's edge and integral values. The transition model contains two transport equations, one for the intermittency, and one for the momentum thickness Reynolds number:

$$\frac{\partial(\rho\gamma)}{\partial t} + \frac{\partial(\rho U_j \gamma)}{\partial x_j} = P_{\gamma 1} - E_{\gamma 1} + P_{\gamma 2} - E_{\gamma 2} + \frac{\partial}{\partial x_j}\left[\left(\mu + \frac{\mu_t}{\sigma_f}\right)\frac{\partial \gamma}{\partial x_j}\right] \quad (1)$$

$$\frac{\partial(\rho\tilde{R}e_{\theta t})}{\partial t} + \frac{\partial(\rho U_j \tilde{R}e_{\theta t})}{\partial x_j} = P_{\theta t} + \frac{\partial}{\partial x_j}\left[\sigma_{\theta t}(\mu + \mu_t)\frac{\partial \tilde{R}e_{\theta t}}{\partial x_j}\right] \quad (2)$$

In equation (1) $P_{\gamma 1}$ and $E_{\gamma 1}$ are transition sources, which are dependend on the local vorticity and several empirical correlations. In addition modifications of the Langtry-correlations have been applied by Geißler[2]. These correlations give the connection between the critical Reynolds number Re_c where intermittency first starts to increase and the transition Reynolds number $Re_{\theta t}$. Another empirical correlation is given for the transition length. The destruction/ relaminarization sources $P_{\gamma 2}$ and $E_{\gamma 2}$ are functions of the vorticity magnitude Ω and ensure that the intermittency remains zero in the laminar boundary layer. The intermittency is always equal one in the free stream.

The source term from equation 2:

$$P_{\theta t} = c_{\theta t}\frac{\rho}{t}(Re_{\theta t} - \tilde{R}e_{\theta t})(1 - F_{\theta t}) \quad (3)$$

forces the transported scalar $\tilde{R}e_{\theta t}$ to match the local value of $Re_{\theta t}$ calculated from an empirical correlation outside the boundary layer. With the blending function $F_{\theta t}$ it is ensured that $P_{\theta t}$ equals zero in the boundary layer. The correlations of Langtry and Menter[5], which have been published recently, can also be used in combination with the present approach for roughness-induced transition.

In this work a third transport equation for the variable called "Roughness Amplification" A_r has been implemented:

$$\frac{\partial(\rho A_r)}{\partial t} + \frac{\partial(\rho U_j A_r)}{\partial x_j} = P_{AR} + \frac{\partial}{\partial x_j}\left[\sigma_{ar}\left(\mu + \mu_t\right)\frac{\partial A_r}{\partial x_j}\right] \quad \text{with:} \quad \sigma_{ar} = 20 \quad (4)$$

The source term P_{AR} produces a transition amplifying variable A_r in close vicinity to a rough wall. Finally, A_r is transported through the flow field by the convective and diffusive terms of equation (4). This behaviour enables the flow history effects to be taken into account. As will be shown by the test case with two-scale roughness height, the roughness-induced amplification of disturbances can show a large lag between the amplification location and the position where the boundary layer reacts to the distortion. This phenomenon is a flow history effect, and can be accounted for by transport equations.

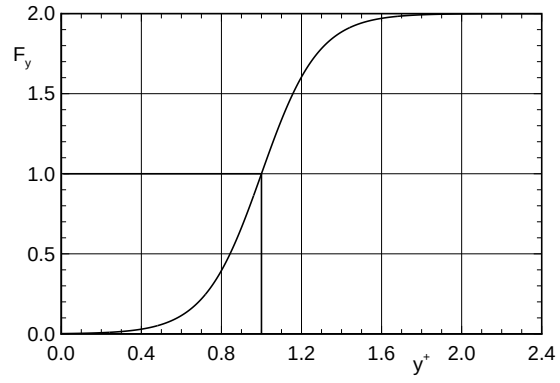

(a) F_y Dependency of y^+

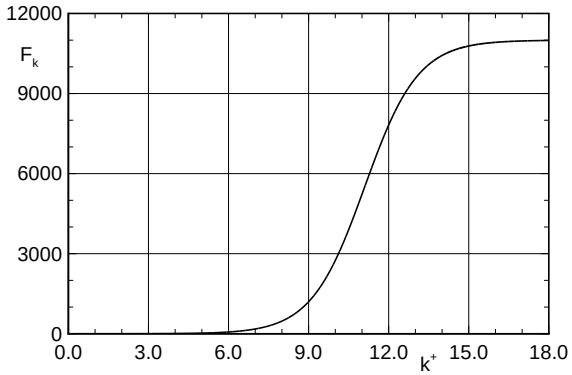

(b) F_k Dependency of k^+

Fig. 1: Generation of A_r in terms of Amp_1 and Amp_2

The source term P_{AR} in equation (4) is applied only to the wall-adjacent cells and is defined as: $P_{AR} = F_y \cdot F_k$. Herein, two equations determining P_{AR} have been calibrated:

$$F_y = \frac{2.0}{1.0 + e^{(-y^+ \cdot 7.0 + 7.0)}} \quad (5)$$

$$F_k = \frac{11000.0}{1.0 + e^{(-k^+ \cdot 1.0 + 11.1)}} \quad (6)$$

The value of P_{AR} in this model depends on the dimensionless wall distance y^+ and the dimensionless roughness k^+ with:

$$y^+ = \sqrt{\frac{\tau_W}{\rho_W}} \cdot \frac{y}{\nu} \quad (7)$$

$$k^+ = \sqrt{\frac{\tau_W}{\rho_W}} \cdot \frac{k_s}{\nu}. \quad (8)$$

As dependency of F_y and F_k, given by equations (5) and (6), the shape of a sigmoid function was chosen with two horizontal asymptotes for k^+, $y^+ \to \pm\infty$. The generation of P_{AR} by k^+ as governed by eq. (6) is shown in fig. 1(b). For hydraulically smooth walls ($k^+ < 5$) there is no production of P_{AR}.

To connect A_r with the transport equation (2), a new variable is defined as follows:

$$Arg_r = max\left(\frac{A_r - 2.0}{2.0}, 0.0\right) \quad (9)$$

$$P_{\theta t} = -10.0 \cdot Arg_r, \text{ if } F_{\theta t} > 0.99. \quad (10)$$

The variable Arg_r ensures that only A_r magnitudes bigger than two and only positive values are considered. With increasing roughness heights and increasing A_r-values the

source term $P_{\theta t}$ becomes negative in order to reduce the transported scalar $\tilde{Re}_{\theta t}$. In this way the transition onset is promoted.

This approach captures the roughness effect on the transition process. The corresponding impact at fully turbulent boundary layers is captured by the boundary condition of the turbulence model as shown in the next section.

3 NUMERICAL METHOD

The numerical simulations have been conducted with the DLR in-house solver TRACE, version 7.0, cf. Nürnberger [10] and Kügeler [4]. In these simulations the Reynolds-averaged Navier-Stokes equations are solved using a finite volume technique. The convective fluxes have been discretized by the 2^{nd} order upwind scheme of Roe [15]. Furthermore, the diffusive fluxes have been discretized by a 2^{nd} order central differencing scheme, where the mixed derivatives are also included ("Full Navier Stokes" approach). These derivatives appear when transforming from the curvilinear to the cartesian frame of reference, and their inclusion leads to accuracy improvement in three-dimensional flows, cf. Röber et al. [14]. The discrete flow equations are iterated towards steady state using an implicit predictor-corrector scheme of Mulder and van Leer[9]. With this scheme, the density residual has been decreased by at least three orders of magnitude for all investigated test cases.

Two equation turbulence model k-ω by Wilcox [20] has been used, together with a dimensionless wall distance of ca. 1 for all simulated test cases. To capture roughness effects in turbulent boundary layers, the boundary condition of the ω-equation at Stokes walls has been corrected as supposed by Wilcox [21]:

$$\omega_{rough} = \frac{u_\tau^2 S_R}{\nu} \quad \text{with:} \quad u_\tau = \sqrt{\frac{\tau_W}{\rho_W}} \quad \text{at:} \quad y = 0 \tag{11}$$

Parameter S_R depends on the surface roughness:

$$S_R = \left(\frac{50}{k^+}\right)^2 \quad \text{for:} \quad k^+ \leq 25 \tag{12}$$

$$S_R = \frac{100}{k^+} \quad \text{for:} \quad k^+ > 25 \tag{13}$$

As compared to the smooth boundary condition:

$$\omega_{smooth} = 10\,\frac{6\nu}{(\beta y)^2} \quad \text{with:} \quad \beta = \frac{3}{40} \quad \text{at:} \quad y = 0 \tag{14}$$

the roughness correction by eq. 11 leads to lower turbulence dissipation rates in the very near wall regions and larger production rates at the beginning of the log-layer, resulting in larger turbulence and viscous loss in the boundary layer. In this way, the roughness effects are reproduced by adjusting the turbulence model's boundary condition only.

4 TEST CASES AND RESULTS

4.1 Flat Plate with Distributed Roughness

The model for roughness induced transition has been calibrated with test cases containing distributed sand grain roughness and linear pressure gradients as reported by Feindt[1].

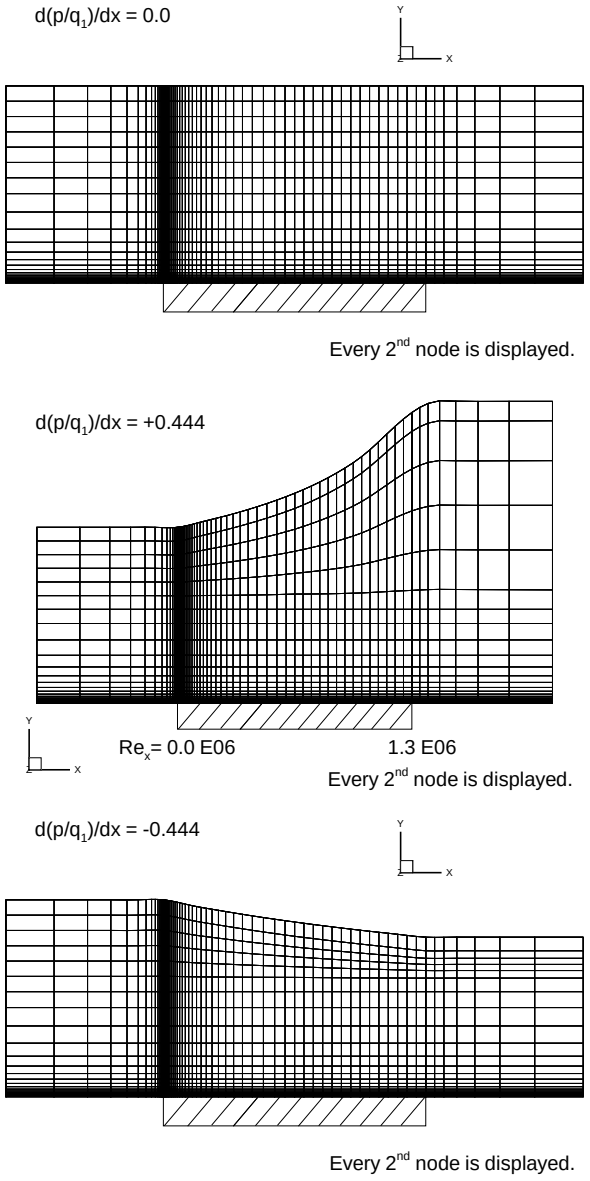

Fig. 2: Feindt's test cases: zero and linear pressure gradients

In Feindt's test case the dependency of transition onset on the roughness height has been measured. With none, expanding and contracting geometries of the outer wall, different linear pressure gradients could be set up. Here, three grids have been generated for simulating the corresponding measurements. All three grids have 8064 cells with 126 cells in x-, and 64 ones in y-direction. With an applied free stream velocity $U_1 = 100\ m/s$ at the beginning of the flat plate the dimensionless wall distance of the first cell y^+ is one in average. With this free stream velocity a shorter flat plate with $x = 0.2\ m$ (Feindt's flat plate length $x = 0.9\ m$), while Reynolds number similarity is given, could be achieved. In this way a faster convergence of our numerical scheme, which favours compressible flows, could be achieved while maintening the physical similarity. The outer wall geometry $r_o(x)$ was calculated by

$$r_o(x) = \sqrt{\frac{r_{o,1}^2}{\sqrt{1.0 - \frac{p_W(x) - p_1}{q_1}}}} \tag{15}$$

with

$$\frac{p_W(x) - p_1}{q_1} = \pm 4.0 \cdot x \tag{16}$$

The outer wall distance at the beginning of the plate is given by

$$r_{o,1}(x = 0\ m) = 0.1495\ m. \tag{17}$$

With this shape of the outer wall a linear pressure gradient was achieved as shown in figure 3. Although there is some difference from Feindt's measurements, there is only a deviation of 3.5 % from the theoretical values, cf. table 1.

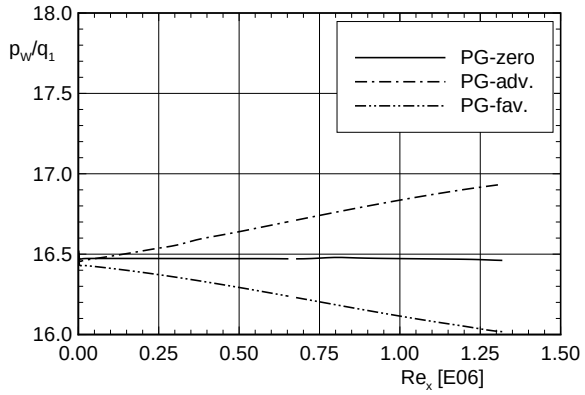

Fig. 3: Linear pressure gradients

PG	$d(p/q_1)/dx$ $[1/m]$		
	theoret.	measured	simul.
zero	0.0	0.0	0.0
adv.	+0.444	+0.371	+0.458
fav.	-0.444	-0.487	-0.430

Tab. 1: Pressure gradients

Six different equivalent sand grain roughness heights have been applied to the flat plate: k_s = 0, 10, 20, 30, 40 and 50 μm. With these values and the kinematic viscosity $\nu = 14.96 \cdot 10^{-6}\ m/s^2$ the same range for the equivalent sand grain roughness height Reynolds number Re_{ks} is achieved like Feindt has applied:

$$Re_{ks} = \frac{U_1 \cdot k_s}{\nu} = 0.0 \ ... \ 334.0. \tag{18}$$

Because the turbulence intensity Tu is not given for the measurements, it was set up in a way that the simulated transition onset with smooth wall is the same as in the experiments. Thus at the beginning of the flat plate the turbulence intensity of $Tu = 1.1$ % has been prescribed.

Figure 4 shows in detail the influence of the "Roughness Amplification" variable A_r on the transition process for the zero pressure gradient test case. On the left hand side the distributions for the smooth wall are shown. There the transition process with no interaction from the third transport equation is demonstrated. The figures on top 4(a) and 4(b) display the contour plot for the transported variable A_r. With no roughness applied $k_s = 0$ μm, the production of A_r is set to zero by equation (9). Otherwise A_r is generated and convected into the flowfield. The contour plots 4(c) and 4(d) display the influence of A_r on the intermittency γ. It can be seen, that the intermittency γ of the Menter and Langtry model is equal zero in the laminar part of the boundary layer, and is equal one in the turbulent boundary layer part and in the free stream. The laminar section with the higher roughness $k_s = 40$ μm is significantly smaller than in figure 4(c). The distributions for Re_θ in figures 4(e) and 4(f) show how much the value for Re_θ is reduced if A_r is generated by equation (10).

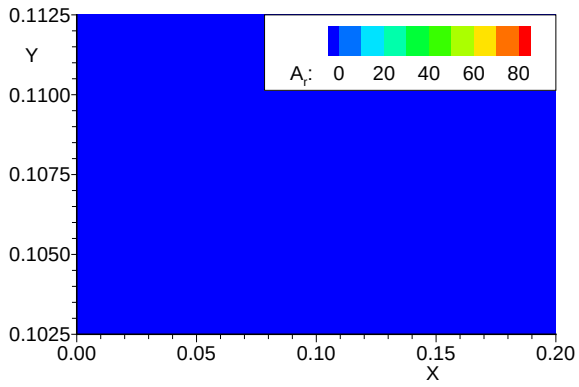

(a) $k_s = 0\ \mu m$

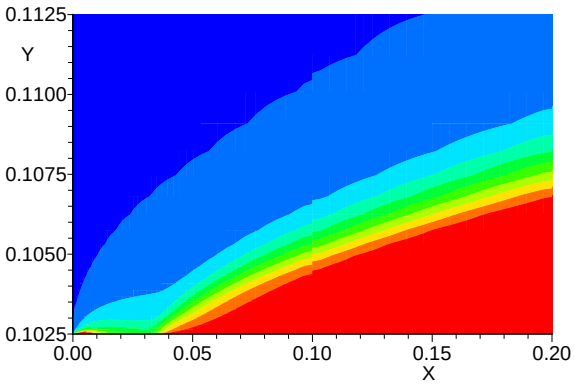

(b) $k_s = 40\ \mu m$

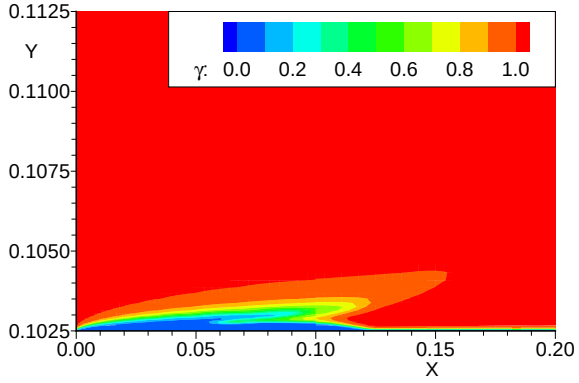

(c) $k_s = 0\ \mu m$

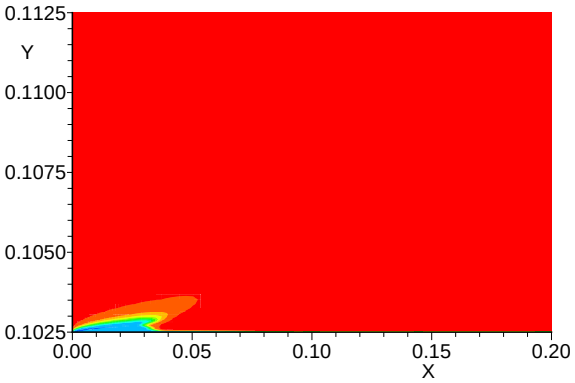

(d) $k_s = 40\ \mu m$

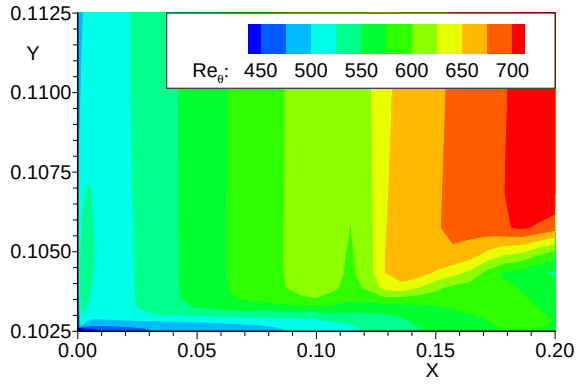

(e) $k_s = 0\ \mu m$

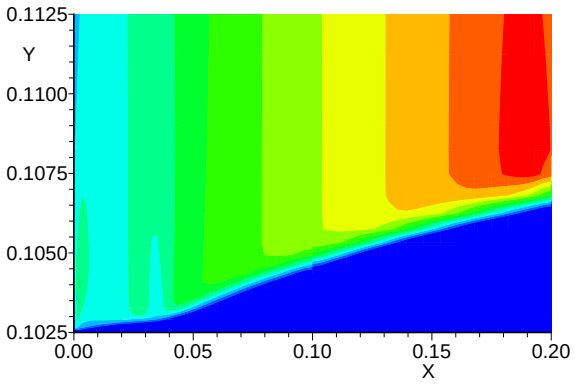

(f) $k_s = 40\ \mu m$

Fig. 4: Distribution of selected values for sand grain roughness heights $k_s = 0\ \mu m$ and $k_s = 40\ \mu m$

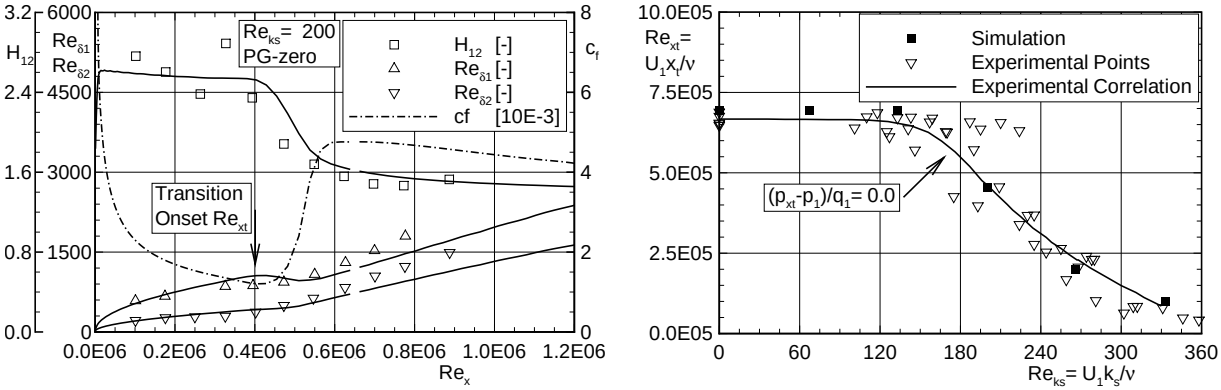

(a) Defining the transition onset Re_{xt} (b) Transition onset Re_{xt} dependency on roughness

Fig. 5: Location of transition onset

The transition onset location Re_{xt} was defined in this work as point of increasing friction coefficient c_f. As example for defining this point figure 5(a) is shown. In the laminar section the displacement and momentum thickness are proportional to $\sqrt{x}$. At the minimum of the friction coefficient the curves of $Re_{\delta 1}$ and $Re_{\delta 2}$ change their shape. For this reason the shape factor $H_{12} = \delta_1/\delta_2$ decreases rapidly (zero pressure gradient) and the transition onset is located at this point. Figure 5(b) shows Feindt's measured transition onset Reynolds numbers Re_{xt} over the equivalent sand grain roughness height Reynolds number Re_{ks} for the zero pressure gradient test case. It seems that the roughness has no influence on the transition onset location if

$$Re_{ks} = \frac{U_1 \cdot k_s}{\nu} < 120.0 \tag{19}$$

that means for hydraulically smooth walls. With increasing Re_{ks} the transition onset is considerably shifted upstream.

The resulting friction coefficients are displayed in figure 6 for the three simulated pressure gradients (PG-zero, PG-adverse and PG-favourable). In figure 6(a) the measured transition onset locations for the zero pressure gradient test case are indicated. These locations have also been introduced in figure 5(b). The plots 6(b) and 6(c) show the curves for the friction coefficient c_f with positive (adverse) and negative (favourable) pressure gradients. It can be seen, that an increasing pressure gradient in the flow direction moves the transition onset location upstream, whereas with a decreasing pressure gradient of the same magnitude the transition does not occur for the equivalent sand grain roughness values $k_s = 0$, 10 and 20 μm.

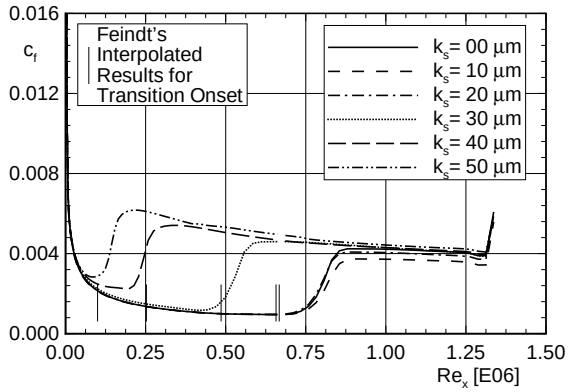

(a) Zero pressure gradient

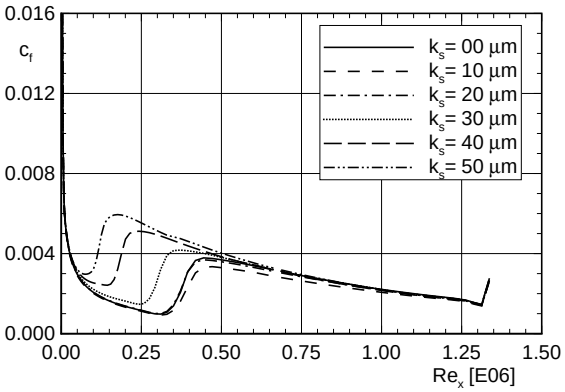

(b) Adverse pressure gradient

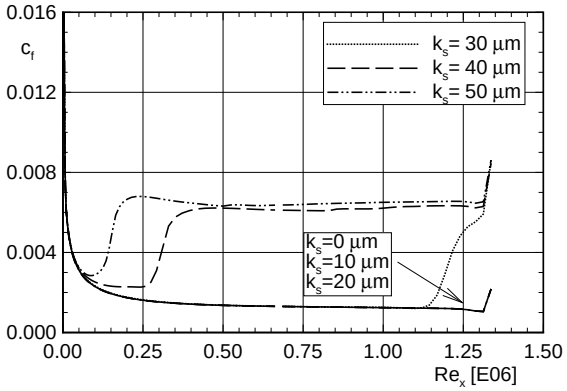

(c) Favourable pressure gradient

Fig. 6: Friction coefficient c_f: zero, linear adverse and favourable pressure gradient

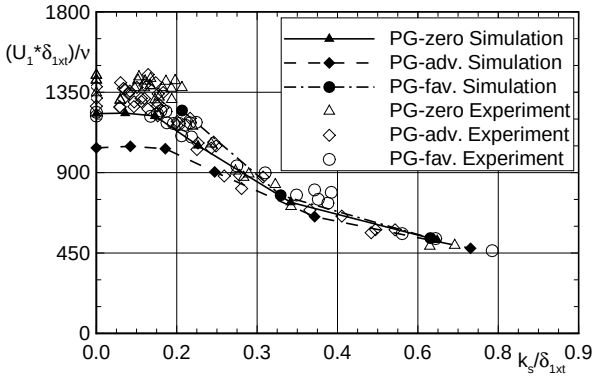

Fig. 7: Influence of roughness on displacement thickness at transition onset

A validation of the prediction of transition onset location with pressure gradients is shown in figure 7. Although the measured values of the displacement thickness at transition onset $(U_1 \cdot \delta_{1xt})/\nu$ does not coincide in on line curve, they seem to build a small range. The simulated values of zero and favourable pressure gradient are inside that range. The predictions of adverse pressure gradients are a bit below the measured values for none or small roughness, indicating a too early transition onset. Since this is hydraulically smooth region, the basic transition model is responsible for the corresponding prediction

deficiency. In general, the agreement between the measured and predicted transition onset Reynolds number of all pressure gradients is very good for increasing roughness heights.

4.2 Flat Plate with Step Change in Roughness

Pinson and Wang[12],[13] report on the effect of a two-scale roughness on boundary layer transition over a heated flat plate. That plate had a full length of 2.05 m. On the first 5 cm a different roughness height was applied than on the remaining downstream 2 m of the plate. The introduced nomenclature determines the applied roughness.

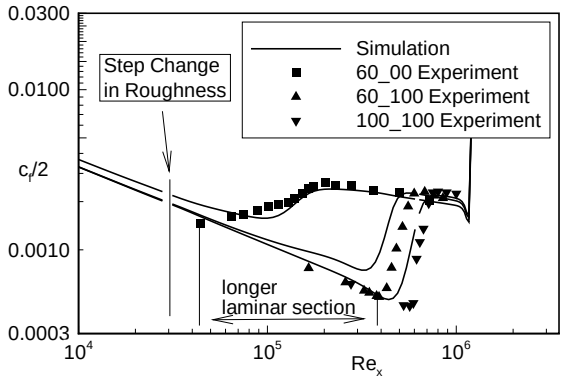

Fig. 8: Friction coefficient c_f with step change in roughness

Sandpaper	Roughness Level		
	R_a	k_s	Re_{ks}
[-]	$[\mu m]$	$[\mu m]$	$[-]$
100	37.0	164	98
60	77.0	341	205

Tab. 2: Roughness levels

According to the nomenclature the test case 100_100 means that there is a constant roughness with 100-grit sandpaper applied to the flat plate. Here, the combinations 60_00, 60_100 and 100_100 are presented. Table 2 gives information about the corresponding roughness heights. The equivalent sand grain roughness was calculated to set the wall boundary condition in TRACE. For this aim following approximation is applied:

$$k_s = 4.433 \cdot R_a \tag{20}$$

For simulations running with that test case a two-dimensional grid has been generated. This grid has 8060 cells with 155 cells in x- and 52 cells in y-direction. The dimensionless wall distance of the cell in close vicinity to the wall is $y^+ \approx 0.8$ in average with a flow velocity $U_1 = 8.6\ m/s$ at the beginning of the plate.
In the experiments the turbulence intensity is given with $Tu = 0.5$ %. A different value of $Tu = 0.8$ % is prescribed in the simulations in order to get the same transition onset location as the smooth wall.

The skin friction coefficients for experiments and simulations are shown in figure 8. The shortest laminar section occurs with the biggest step change in roughness in test case 60_00. A detailed view on this test case is shown in figure 9. It has been simulated

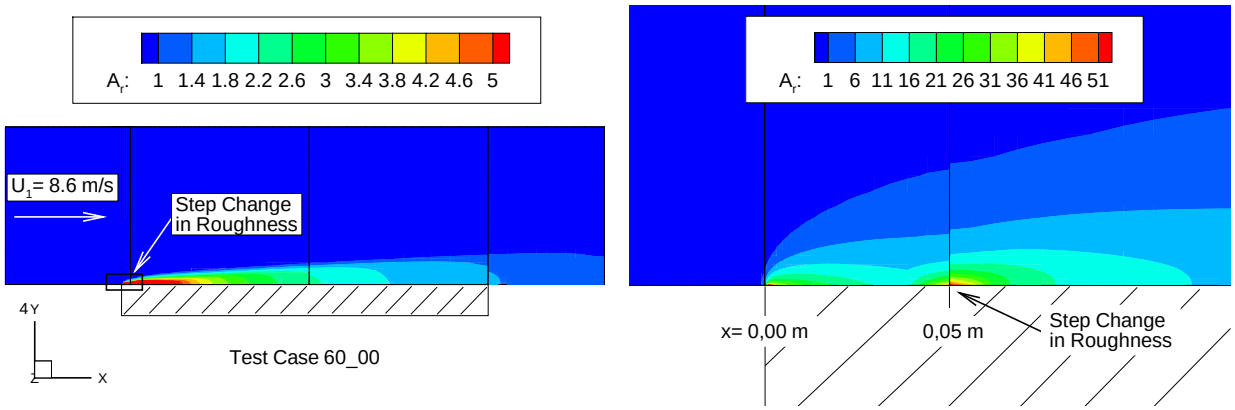

(a) Flowfield (b) Detail view on step in roughness

Fig. 9: Generation of amplifiying variable A_r with step change in roughness

while adding a constant value of $A_r = 3000$ in the two cells which are in close vicinity to the step. Figure 9(a) shows the whole flowfield for that test case and figure 9(b) zooms in on the step. Interestingly, the laminar section can be extended if a small roughness behind the step is added, cf. figure 8. This effect is traced back to the fact, that the formation and amplification of flow disturbances is reduced due to a smaller step height. The information of this smaller step (60_100) is transported through the flowfield, since the roughness amplification variable A_r is handled by a transport equation in the present approach. In other words, the impact at the flow is manifested somewhere else (at the transition location) than the origin of the disturbance (at the step location). Thus the transition occurs earlier than in the test case with constant roughness (100_100), but later than in the case with the large step (60_00); an effect which is accurately reproduced by the roughness-induced transition model.

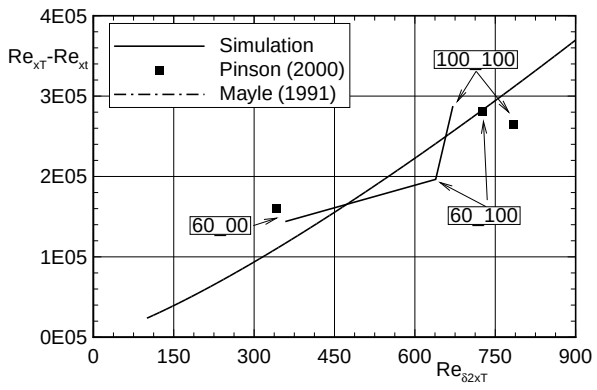

Fig. 10: Comparison of the transition length with Mayle's smooth-wall correlation[6]

The prediction of the transition length, expressed by $Re_{xT} - Re_{xt}$ in figure 10 (t-transition onset, T-transition end), is in reasonable agreement with the experiments and also with the smooth-wall correlation of Mayle[6]:

$$Re_{xT} - Re_{xt} = 75.0 \cdot (Re_{\delta 2xT})^{5/4} \qquad (21)$$

It seems that the surface roughness can considerably shift the transition onset location, but that it does not alter the transition length significantly.

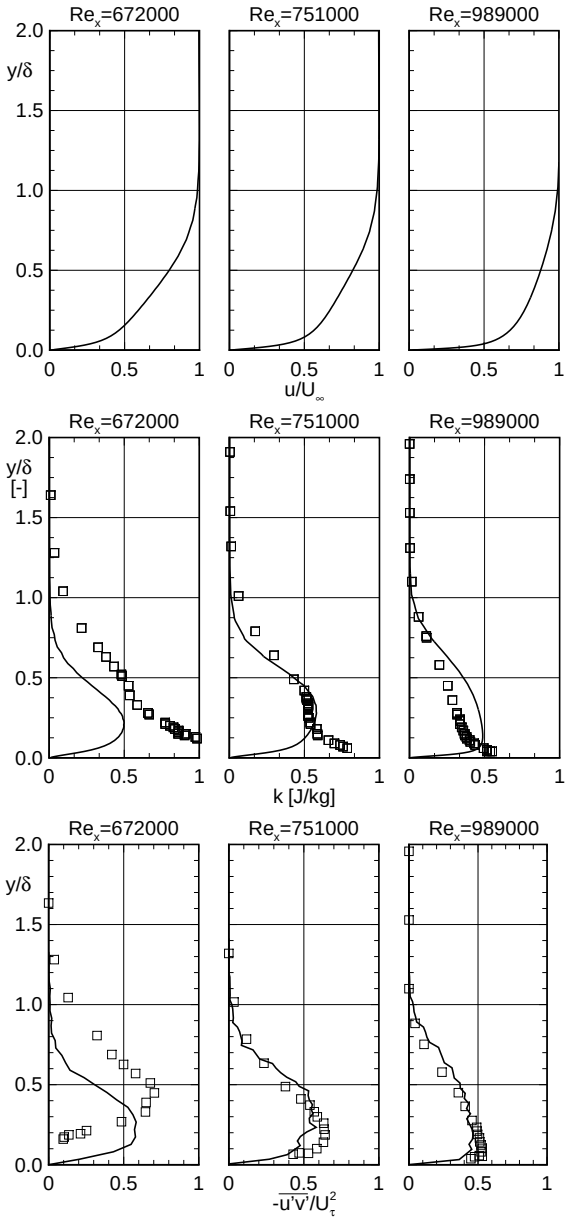

Fig. 11: Selected distributions of turbulent quantities for 100_100 case at $8,6\ m/s$

The figure 11 shows velocity u/U_∞, turbulent kinetic energy:

$$k = 0.5 \cdot \left(\overline{u'^2} + \overline{v'^2} + \overline{w'^2}\right) \tag{22}$$

and Reynolds shear stress $-\overline{u'v'}/U_\tau^2$ profiles for the boundary layer at selected Re_x-positions of the constant roughness test case 100_100. Although Pinson reports only u'/U_∞ and v'/U_∞ values for calculating the turbulent kinetic energy k, the rough but useful assumption

$$u' : v' : w' = 4 : 2 : 3 \tag{23}$$

was made, cf. Wilcox[21]. This assumption is valid for fully turbulent flows and was nearly achieved at $Re_x = 989000$ with $u'/v' = 2.5$ in average. Thus the arithmetic mean between u' and v' was taken for w'.

With the eddy viscosity μ_t the Reynolds shear stress $-\overline{u'v'}$ is calculated:

$$-\overline{u'v'} \;=\; \frac{\mu_t}{\rho}\left(\frac{\partial u}{\partial y}\right) \tag{24}$$

The first streamwise position is located at the end of the transitional region, and the both other positions are clearly located in the fully turbulent part. The former position shows some deviations between the measured and simulated values, especially for the wall distance of the maximum turbulent kinetic energy. The reason therefore is the large sensitivity of the transitional boundary layer with respect to the transition onset point. Due to a somewhat early onset prediction, the simulation suggest already a fully turbulent boundary layer at this streamwise position, with turbulence quantities shifted towards the wall. The deviation is much smaller for the both downstream positions, since the aforementioned sensitivity is much smaller in the fully turbulent boundary layer. The very good agreement between the simulation and experiment for the downstream positions confirms the ability of the method for the prediction of roughness-induced transitional boundary layers.

5 CONCLUSIONS AND OUTLOOK

A model for prediction of the roughness-induced transition has been implemented in the DLR flow solver TRACE using only local variables. This approach is based on the γ-θ-transition model of Menter and Langtry[7] and includes a new transport equation for a roughness-induced amplification of flow disturbances. The roughness amplification is applied only to the wall-adjacent cells, and is transported by the convective and diffusive terms of the transport equation into the complete flow field. Validation on flat plates with pressure gradients, constant and two-scale roughness has been made. Results clearly demonstrate the feasibility of the current approach. In agreement with the measurements the transition onset position is shifted when different surface roughness values and step change of roughness are prescribed. It seems that the surface roughness can considerably shift the transition onset location, but that it does not alter the transition length significantly.

Further work needs to be done on flow situations with more than three (roughness height, pressure gradient, step change in roughness) parameters acting on the flow. To predict the roughness effects in complex, three-dimensional flows, the wall curvature, flow separations, unsteady flow, etc. have to be considered.

6 ACKNOWLEDGMENTS

First of all, the authors would like to gratefully acknowledge the support of the TRACE team from the DLR Institute of Propulsion Technology (Cologne, Germany), in particular Dr. E. Kügeler, who did a lot of work in numerical implementation of the transport equation. Furthermore, we take this opportunity to thank Ms. K. Geißler from MTU Aero Engines (Munich, Germany) for providing the correlation functions of the transition model and Mr. E. Lewin from TU Braunschweig, Institut of Fluid Mechanics (Brunswick, Germany) for his help in setting up the test cases and programming issues.

The development work was conducted as a part of the joint research programme COORETEC-turbo in the frame of AG Turbo. The work was supported by the Bundesministerium für Wirtschaft und Technologie (BMWi) as per resolution of the German Federal Parliament under grant number 0327715H. The authors gratefully acknowledge AG Turbo, MTU Aero Engines and DLR for their support and permission to publish this paper. The responsibility for the content lies solely with its authors.

7 NOMENCLATURE

$c_f = \tau_W / q_1$	$[-]$	Friction Coefficient
k	$[J/kg]$	Turbulent Kinetic Energy per Unit Mass, cf. Eq. (22)
k_s	$[m]$	Equivalent Sand Grain Roughness Height
k^+	$[-]$	Dimensionless Roughness Height, cf. Eq. (8)
$q_1 = p_{t1} - p_1$	$[Pa]$	Dynamic Pressure At Inlet
t	$[s]$	Time
$\overline{u'v'}$	$[m^2/s^2]$	Reynolds Shear Stress
$x,\ y,\ z$	$[m]$	Cartesian Coordinates
y^+	$[-]$	Dimensionless Wall Distance, cf. Eq. (7)
A_r	$[-]$	Transported Variable "Amplifying Roughness"
P	$[-]$	Source Term
E	$[-]$	Destruction Term
R_a	$[m]$	Arithmetic Average Roughness Height
Re_{ks}	$[-]$	Equivalent Sand Grain Roughness Height Reynolds Number, cf. Eq. (18)
$Re_x = U_1 x / \nu$	$[-]$	Reynolds Number
$Re_{xt} = U_1 x_t / \nu$	$[-]$	Reynolds Number at Transition Onset
$Re_{xT} = U_1 x_T / \nu$	$[-]$	Reynolds Number at Onset of Turbulence Boundary Layer
$Re_{\theta t} = U_\infty \theta_t / \nu$	$[-]$	Local Transition Onset Momentum Thickness Reynolds Number (Based On Free Stream Conditions)
$\tilde{Re}_{\theta t}$	$[-]$	Local Transition Onset Momentum Thickness Reynolds Number (Obtained From Transport Equation)
Tu	$[-]$	Turbulence Intensity
U_1	$[m/s]$	Velocitiy at Beginning of Flat Plate
$U_\tau = \sqrt{\tau_W / \rho_W}$	$[m/s]$	Shear Velocitiy
γ	$[-]$	Intermittency
δ	$[m]$	Boundary Layer Thickness
δ_1	$[m]$	Displacement Thickness
δ_2	$[m]$	Momentum Thickness (θ as Subscript)
ρ	$[kg/m^3]$	Density
μ	$[kg/(ms)]$	Dynamic Viscosity
μ_t	$[kg/(ms)]$	Eddy Viscosity
$\nu = \mu / \rho$	$[m^2/s]$	Kinematic Viscosity
$\tau_W = \rho_W \nu (\partial u / \partial y)_W$	$[kg/(ms^2)]$	Wall Shear Stress

REFERENCES

[1] E. G. Feindt, Untersuchungen über die Abhängigkeit des Umschlages laminar-turbulent von der Oberflächenrauhigkeit und der Druckverteilung, *DFL Bericht*, **43** (1956)

[2] K. Geißler, Improved Reproduction of RANS Simulations with Two Additional Partial Differential Equations for Intermittency and Transition Onset Reynolds Number for the Test Data of Highly Loaded Turbine Cascades at Low Reynolds Numbers, *Diploma Thesis*, Technische Universität Dresden, Institut für Strömungsmechanik, **D 1699** (2009)

[3] F. Hummel, M. Lötzerich, P. Cardamone, L. Fottner, Surface Roughness Effects on Turbine Blade Aerodynamics, *Journal of Turbomachinery* **Vol. 127** (2005)

[4] E. Kügeler, Numerisches Verfahren zur genauen Analyse der Kühleffektivität filmgekühlter Turbinenschaufeln, *DLR Forschungsbericht* **2005–11** (2005)

[5] R. B. Langtry, F. R. Menter, Correlation-based transition modeling for unstructured parallelized computational fluid dynamics codes, *AIAA Journal*, **Vol. 47, No. 12, pp. 2894–2906** (2009)

[6] R. E. Mayle, The Role of Laminar Turbulent Transition in Gas Turbine Engines, *ASME Paper*, **No. 91–GT–261** (1991)

[7] F. R. Menter, R. B. Langtry, S. R. Likki, Y. B. Suzen, P. G. Huang, S. Völker, A Correlation-Based Transition Model Using Local Variables. Part 1 - Model Formulation, *ASME Paper*, **No. GT2004–53452** (2004)

[8] F. R. Menter, R. B. Langtry, S. R. Likki, Y. B. Suzen, P. G. Huang, S. Völker, A Correlation-Based Transition Model Using Local Variables. Part 2 - Test Cases and Industrial Applications, *ASME Paper*, **No. GT2004–53454** (2004)

[9] W. A. Mulder, B. van Leer, Implicit Upwind Methods for the Euler Equations, *AIAA Paper*, **No. 83–1930** (1983)

[10] D. Nürnberger, Implizite Zeitintegration für die Simulation von Turbomaschinenströmungen, PhD-Thesis, Ruhr-Universität Bochum, *DLR Forschungsbericht* **2004–27**, (2004)

[11] H. Oertel Jr., J. Delfs, Strömungmechanische Instabilitäten, *Springer*, **ISBN 3–540356984–7**, Berlin (1996)

[12] M. W. Pinson, T. Wang, Effect of Two Scale Roughness on Boundary Layer Transition Over a Heated Flat Plate: Part 1 - Surface Heat Transfer, *Journal of Turbomachinery*, **Vol. 122, pp. 301–307** (2000)

[13] M. W. Pinson, T. Wang, Effect of Two Scale Roughness on Boundary Layer Transition Over a Heated Flat Plate: Part 2 - Boundary Layer Structure, *Journal of Turbomachinery*, **Vol. 122, pp. 308–316** (2000)

[14] T. Röber, D. Kožulović, E. Kügeler, D. Nürnberger, Appropriate turbulence modelling for turbomachinery flows using a two-equation turbulence model, in: *New Results in Numerical and Experimental Fluid Mechanics V*, **pp. 446–454**, Eds.: H. J. Rath et al., Springer, Berlin (2006)

[15] P. Roe, Approximate Riemann solvers, paramter vector and difference schemes, *J. Comp. Phys.*, **Vol. 34, pp. 357–372** (1981)

[16] H. Schlichting, Experimentelle Untersuchungen zum Rauhigkeitsproblem, *Ingenieur-Archiv*, **VII. Band, 1. Heft, S. 1–34**, (1936)

[17] K. Standish, P. Rimmington, J. Laursen, H. N. Paulsen, Computational Prediction of Airfoil Roughness Sensitivity, *AIAA Paper*, **AIAA 2010–460** (2010)

[18] M. Stripf, A. Schulz, H.-J. Bauer, S. Wittig, Extended Models for Transition Rough Wall Boundary Layers With Heat Transfer - Part I: Model Formulation, *Journal of Turbomachinery*, **Vol. 131** (2009)

[19] M. Stripf, A. Schulz, H.-J. Bauer, S. Wittig, Extended Models for Transition Rough Wall Boundary Layers With Heat Transfer - Part II: Model Validation and Benchmarking, *Journal of Turbomachinery*, **Vol. 131** (2009)

[20] D. C. Wilcox, Reassessment of the scale-determining equation for advanced turbulence models, *AIAA Journal*, **Vol. 26, No. 11, pp. 1299–1310** (1988)

[21] D. C. Wilcox, Turbulence Modeling for CFD, *DCW Industries*, **Second Edition**, La Canada, California (1998)